Applied Physics Express

LETTER

Faraday rotator based on a silicon photonic crystal slab on a bismuth-substituted yttrium iron garnet thin film

To cite this article: Siyuan Gao *et al* 2023 *Appl. Phys. Express* **16** 072003

Applied Physics Express **16**, 072003 (2023) LETTER
https://doi.org/10.35848/1882-0786/acdc81

Faraday rotator based on a silicon photonic crystal slab on a bismuth-substituted yttrium iron garnet thin film

Siyuan Gao[1*], Yasutomo Ota[2*], Tianji Liu[3], Feng Tian[1], and Satoshi Iwamoto[1]

[1]*Research Center for Advanced Science and Technology, The University of Tokyo, Meguro, Tokyo 153-8904, Japan*
[2]*Department of Applied Physics and Physico-Informatics, Keio University, Yokohama, Kanagawa 223-8522, Japan*
[3]*GPL Photonics Laboratory, State Key Laboratory of Luminescence and Applications, Changchun Institute of Optics, Fine Mechanics and Physics, Chinese Academy of Sciences, Changchun, Jilin 130033, People's Republic of China*

*E-mail: gaosy@iis.u-tokyo.ac.jp; ota@appi.keio.ac.jp

Received April 24, 2023; revised May 9, 2023; accepted June 7, 2023; published online July 11, 2023

We report the design of an ultrathin Faraday rotator consisting of a silicon photonic crystal (PhC) slab on a bismuth-substituted yttrium iron garnet (Bi:YIG) thin film. By directing light into guided modes in the Bi:YIG layer via diffraction in the PhC layer, we numerically demonstrate a Faraday rotation angle of ~45° at a telecom wavelength with a Bi:YIG layer thickness of only ~500 nm. This structure permits a high light transmittance of about 70%, enabled by electromagnetically induced transparency. The proposed design only requires nanopatterning of the Si layer, providing a viable route to practical ultrathin Faraday rotators.

Faraday rotators rotate the linear polarization of light passing through them and are an essential element of many nonreciprocal free-space optics including Faraday isolators, circulators, and mirrors. In general, Faraday rotators tend to be bulky in the optical regime due to the weak magneto-optical (MO) effects of transparent materials.[1,2] The miniaturization of Faraday rotators has been a fascinating research direction for expanding their applications. A straightforward approach is to enhance light–matter interactions in the constituent MO materials by using optical resonances in photonic micro/nanostructures such as one-dimensional[3–5] and two-dimensional photonic crystals (PhCs),[6,7] and plasmonic structures.[8–15] However, the observed Faraday rotation angles (θ_F) were far less than the ideal value of 45°, with which an ideal Faraday isolator can be built, and the measured light transmittances (T) were rather low[11–14,16] limiting their use in nonreciprocal free-space optics based on light polarization.

All-dielectric MO metasurfaces have recently emerged as an alternative route to realize ultrathin Faraday rotators.[17–20] By judiciously arranging the array of resonant structures made from a MO material, a high T of 96% and a moderate θ_F of 7.6° have been numerically demonstrated in a single-layer structure.[21] The performance is not sufficient for practical use but the MO structure appears promising with further optimizations.[22] However, the MO materials considered in the metasurfaces are iron garnets, which are notoriously intractable to nanopatterning. Forming vertical sidewalls in the constituent garnet resonators is considered critical for achieving the designed performance[23] but has been known to be very challenging.[24]

More recently, S. Xia et al. proposed and demonstrated another approach to realize an all-dielectric MO metasurface without nanopatterning of the iron garnet layer.[25] They formed an array of microdisk resonators made from amorphous silicon on top of an unpatterned Ce:YIG thin film and observed a ~ fourfold enhancement of θ_F in comparison with a plane MO material of the same thickness. This approach wisely avoids direct nanopatterning of the garnet material and shows great potential for the faithful fabrication of the designed optical structure. However, the hybrid MO structure only exhibits a small θ_F of less than 1° even in the design, which will hinder its use as a practical Faraday rotator. The same issue is found for the hybrid MO metasurfaces using ferromagnetic metals.[22,23,26]

In this study, we report the design of an all-dielectric hybrid MO nanostructure consisting of a silicon-based photonic crystal (PhC) on a bare bismuth (Bi)-substituted yttrium iron garnet (Bi:YIG) thin film. Nanoholes are perforated only in the Si layer so that the Bi:YIG layer remains intact. We found high Q factor modes, which originated from guided mode resonances (GMRs) and are supported mainly in the Bi:YIG layer, significantly enhances Faraday rotation in the structure. After fine-tuning the structure, a design based on a 500 nm thick Bi:YIG thin film exhibits a θ_F of ~45° with a high T of ~70% at ~1.5 μm wavelength.

Figure 1(a) shows the hybrid MO structure considered in this study. The structure consists of a Si-based PhC slab on a Bi:YIG film with a submicron thickness (h_{yig}). The whole structure is embedded in a SiO_2 matrix with a refractive index of 1.45. The YIG layer is described by a relative permittivity tensor $\varepsilon = [\epsilon, ig, 0; -ig, \epsilon, 0; 0, 0, \epsilon]$ under an external magnetic field along the z-axis. We used the experimentally-measured values of $\epsilon = 2.4^2$ and $g = 0.00235$ for a commercially available Bi:YIG substrate in the telecom wavelength band. The PhC structure is assumed to be made from a monocrystalline silicon slab ($n_{Si} = 3.45$) with a thickness of $h_{Si} = 160$ nm. Our design of the Si PhC starts from a square array of circular perforated holes with a diameter $a = 325$ nm. We modify the circular nanoholes to elliptical ones with the length of the long axis b in the way shown in the inset of Fig. 1(b). The primitive unit cell of the structure after the modification is shown in Fig. 1(b). The period of the PhC is fixed to be $P = 880$ nm. The strength of the structural modification is quantified with a parameter $\delta = b - a$. Numerical analyses were performed with electromagnetic simulations using COMSOL Multiphysics. We set periodic boundary conditions in the x and y directions and perfectly matched layers at the upper and lower boundaries along the z direction. To evaluate θ_F and T, the structure is vertically illuminated from 6 μm above with x-polarized light propagating along the z direction and optical responses are evaluated at 6 μm below the structure.

First, we investigated optical resonances supported in the hybrid optical structure. Figure 2(a) shows computed

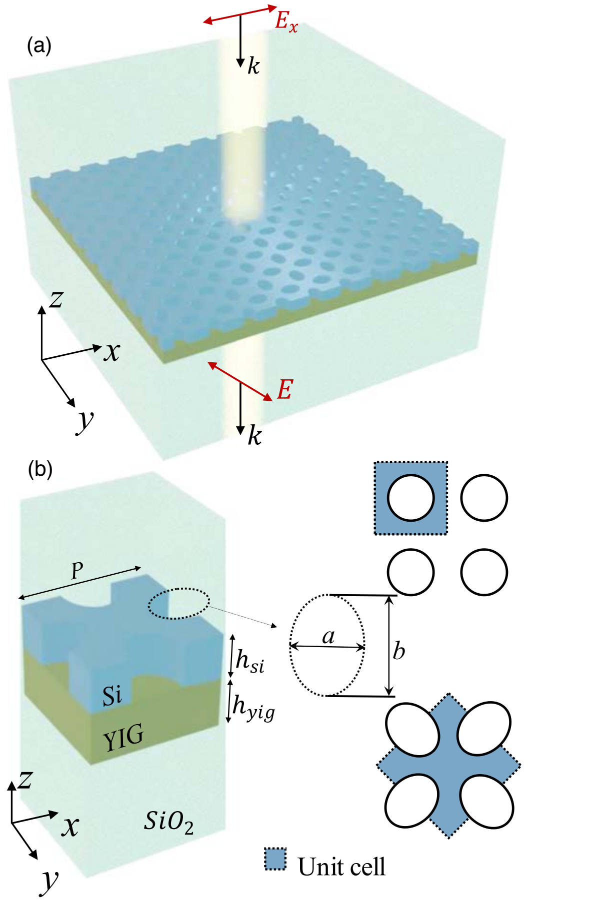

Fig. 1. (a) Investigated hybrid MO nanostructure. A Si PhC slab is placed on an unstructured Bi:YIG thin film. The entire structure is embedded in SiO_2. (b) Unit cell of the structure with notes on the design parameters. The right inset shows the modification of the nanoholes from circular to elliptical.

transmission spectra for the structure with $h_{yig} = 450$ nm when varying δ. When $\delta = 0$ nm, we observed two broad resonance dips in the spectrum. They originated from electric-dipole-like (ED-like) and magnetic-dipole-like (MD-like) resonances mainly supported in the Si layer. Figures 2(b) and 2(c) show the field distributions of the MD-like and ED-like modes. The two kinds of resonances are, respectively, doubly degenerated owing to the C_{4v} symmetry of the structure. When $\delta \neq 0$ nm, two additional resonance dips appear in the spectra. They are associated with TE-like and TM-like GMRs supported mainly in the Bi:YIG layer. The asymmetric resonance shapes originate from Fano resonance.[24,25] Figures 2(d) and 2(e) show the field distributions of the TM-like and TE-like GMRs. Analogous to the dipole-like resonances, the GMRs are also, respectively, doubly degenerated. The corresponding guided modes originally exist below the light line and respond to the incident light only when they have finite coupling to free-space modes.

We found that δ serves as a tuning knob for the coupling between the incident light and the GMRs. The coupling vanishes when $\delta = 0$ nm and gradually increases with increasing δ, as evidenced in the spectra shown in Fig. 2(a). This behavior is also confirmed from computed Q factors of the GMRs as shown in Fig. 2(f). We observed the diverging of the Q factor when approaching $\delta = 0$ nm and its rapid decrease

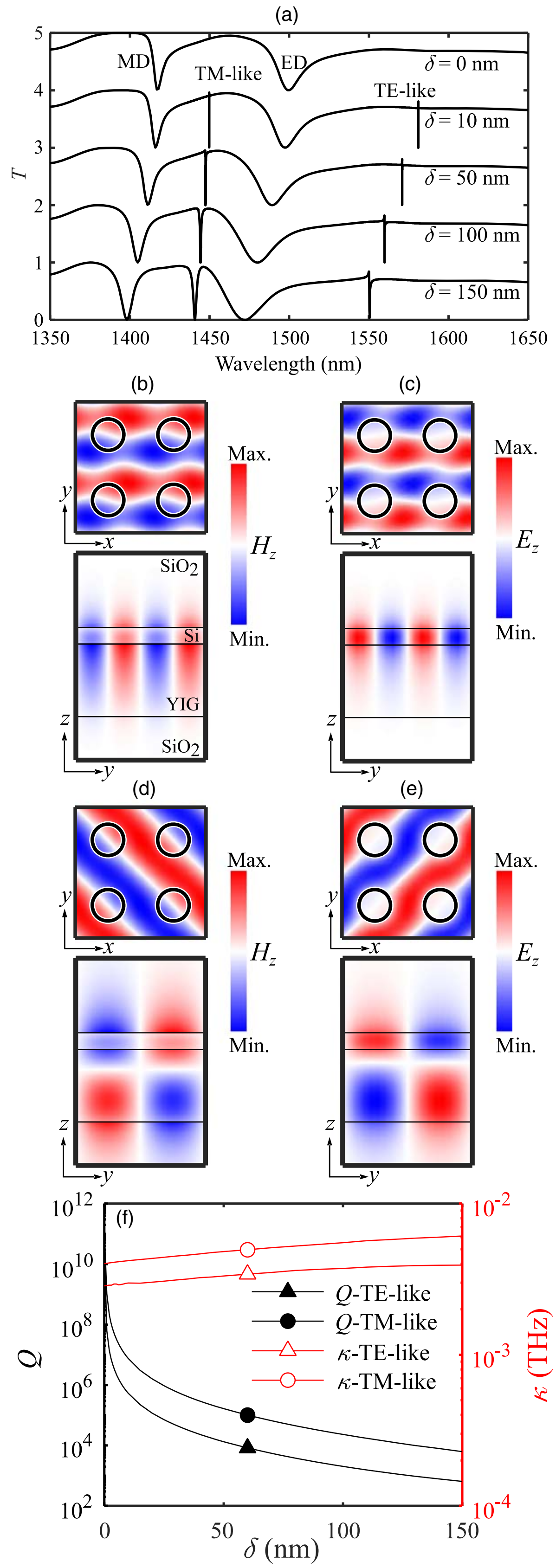

Fig. 2. (a) Simulated transmittance spectra of the all-dielectric MO metasurfaces designed with different δ s, while fixing $P = 880$ nm, $a = 325$ nm, $h_{yig} = 450$ nm and $h_{si} = 140$ nm. Field distributions of (b) the ED-like and (c) MD-like modes. The top panels show field slices in the middle of the Si PhC slab. The bottom panels show cross sections. Field distributions of (d) the TE-like and (e) TM-like modes. (f) Computed Q factors and MO coupling strengths of the GMRs when varying δ.

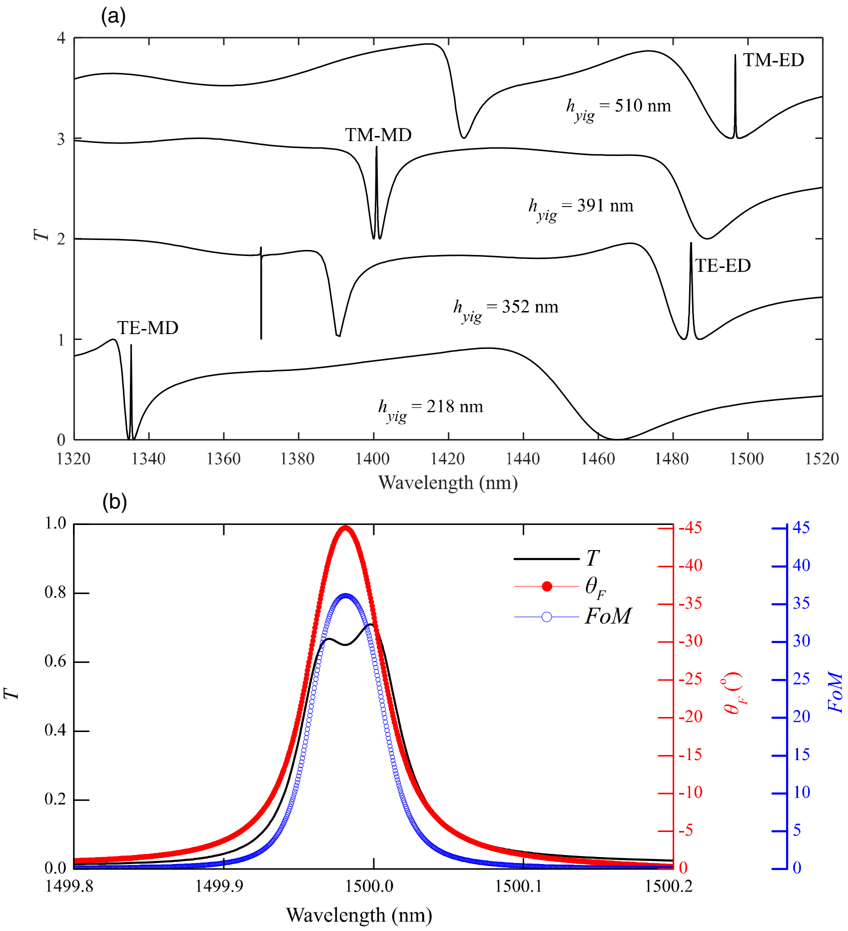

Fig. 3. (a) Transmission spectra under the four different EIT conditions obtained by tuning h_{yig} . $P = 880$ nm, $a = 325$ nm, $\delta = 15$ nm, and $h_{si} = 140$ nm are fixed. (b) Transmission, θ_F and FoM spectra for the structure realizing the EIT of the TE-like GMR overlapped with the ED-like modes. δ was finely tuned to be 15 nm to attain a θ_F of ~45°. h_{yig} was set to 513 nm to assure the exact EIT condition.

for nonzero δ. The resilience of the GMRs to the Si PhC of $\delta = 0$ nm can be associated with symmetry-protected bound states in the continuum (BIC).[24,25,27] In this interpretation, the situation with $\delta \neq 0$ nm can be regarded as the case that a quasi-BIC mode in the Si PhC mediates the coupling of incident light with the GMRs. More changing the airhole shape by increasing δ, stronger free-space coupling and thus a lower Q factor of the GMRs was realized in the structure. An interesting note is that the field distributions of the involved optical modes do not largely change when varying δ. Indeed, MO coupling strengths, κ, which are calculated from the field distributions,[28] do not alter largely even when assuming a large δ, as shown in Fig. 2(f). Since θ_F can be assumed to be proportional to $Q \cdot \kappa$,[21] the observed decoupling of κ from Q will simplify the design process of the Faraday rotators. In other words, we can design θ_F to be $\sim 45°$ simply by controlling the Q factor of the GMRs via modifying δ.

Next, we discuss the design strategy for simultaneously achieving the ideal θ_F and a high T. As mentioned just above, we can finely tune θ_F by controlling the Q factor of the GMRs with δ. Thus, the remaining challenge is to realize a high T in the structure under concern. To this end, we exploit electromagnetically induced transparency (EIT)[29–33] or the Kerker effect,[34–36] which turns transmission dips into peaks and can be activated by spectrally overlapping optical resonances. For mutual spectral tuning of the relevant optical modes, we employ h_{yig} as a controlling parameter. Figure 3(a) shows computed transmission spectra for four different values of h_{yig} when $\delta = 30$ nm. Reflecting the different origins of the modes, only the GMRs exhibit a large shift of the resonant wavelengths, while those of the dipole-like modes are much smaller. The four values of h_{yig} correspond to the situations realizing the spectral overlaps between one of the GMRs and a dipole-like mode. For all four situations, sharp spectral peaks (rather than dips) of the GMRs are observed within broader dipole resonances, as intended.

Figure 3(b) shows a spectrum for the case where TM-like GMRs are resonant with the ED-like modes at the wavelength of ~1.5 μm. In this particular instance, we further tailored δ to be 15 nm for achieving $\theta_F \sim 45°$, and h_{yig} to be 513 nm for the reassurance of the exact EIT condition. The red curve shows the spectrally resolved θ_F, which reaches 45° at the maximum, which is 800 times larger than that of a fully magnetized bare Bi:YIG film of the same thickness. The black curve shows a corresponding transmission spectrum. A high T of 65% is achieved at the wavelength of the θ_F peak. The observed spectral doublet stems from the spectral splitting due to the MO coupling between the two orthogonal TM-like GMRs. The plot also includes a curve of a figure of merit (FoM) of this device, defined as $\sqrt{T}|\theta_F|$. The maximum FoM is over 36, which is more than 200 times larger compared with that in the previous study applying silicon resonator arrays on Ce:YIG thin films.[25]

Finally, we investigated the influence of the device size on its performance. Since we employed GMRs, the device size in the

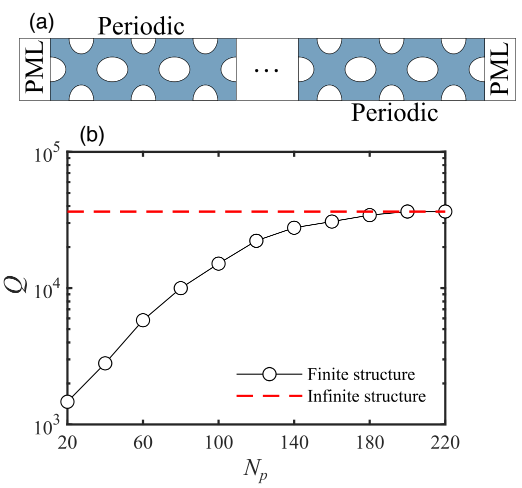

Fig. 4. TM-like GMR in finite structures. (a) Simulation model of the finite PhC structure under consideration. Periodic boundaries are defined along the y direction. The structure in the x direction contains a finite number of periods (N_p) and is terminated by PML layers. (b) Evolution of Q factors when increasing N_p.

lateral directions will be an essential factor in determining the Q factors of the resonances. Meanwhile, the numerical calculations presented so far were obtained by assuming infinitely large structures by setting the periodic boundary conditions. In the following, we show the results obtained by replacing the periodic boundaries for the x computation domain edges with absorbing boundaries described by perfectly matched layers. The setup under concern is schematically shown in Fig. 4(a). We consider here the Faraday rotator structure designed in Fig. 3(b). Figure 4(b) shows a computed evolution of Q factor of a TM-like GMR when changing the number of periods (N_p) in the x direction. As anticipated, the Q factor is significantly limited for the structure with a small N_p. However, the Q factor grows exponentially when increasing N_p and shows a saturation around the value of the infinitely large structure when around $N_p = 200$. This result indicates that the designed structure will properly function when incorporating a large enough N_p over 200 in the structure. When $N_p = 200$, the lateral device size will be about 180 μm, a realistic length for the actual device fabrication using conventional lithography techniques.

In conclusion, we numerically demonstrated an ultrathin Faraday rotator structure that simultaneously achieves a θ_F of 45°, high T of 65% and high FoM of 36 at a telecom wavelength of 1.5 μm. The design is based on a hybrid MO structure consisting of a Si PhC slab on a 513 nm thick Bi:YIG film. For ease of device fabrication, only the Si layer is nanopatterned, leaving the Bi:YIG layer unstructured. The large Faraday rotation was obtained through coupling incident light into the GMRs by tuning the degree of asymmetry of the PhC structure. The high T was achieved through EIT by spectrally overlapping the GMRs and low-Q dipole-like resonances. We also investigated the influence of the device size on its performance and showed that an N_p over 200 is sufficient for the Faraday rotator to function properly. The device design proposed here will expedite the realization of pragmatic ultrathin Faraday rotators, which hold substantial promise for applications in free-space nonreciprocal MO devices including MO sensors and modulators.

Acknowledgments This work was supported by KAKENHI (17H06138, 19K05300, 22H00298, 22H01994 and 22K18989), JST CREST (JPMJCR19T1), JST FOREST Program (JPMJFR213F), and Nippon Sheet Glass Foundation.

1) T. Tepper and C. A. Ross, J. Cryst. Growth **255**, 324 (2003).
2) G. Schmidt, C. Hauser, P. Trempler, M. Paleschke, and E. Th. Papaioannou, Phys. Status Solidi B **257**, 1900644 (2020).
3) M. Inoue, K. Arai, T. Fujii, and M. Abe, J. Appl. Phys. **85**, 5768 (1999).
4) A. B. Khanikaev, A. B. Baryshev, P. B. Lim, H. Uchida, M. Inoue, A. G. Zhdanov, A. A. Fedyanin, A. I. Maydykovskiy, and O. A. Aktsipetrov, Phys. Rev. B **78**, 193102 (2008).
5) M. A. Kozhaev, A. I. Chernov, D. A. Sylgacheva, A. N. Shaposhnikov, A. R. Prokopov, V. N. Berzhansky, A. K. Zvezdin, and V. I. Belotelov, Sci. Rep. **8**, 11435 (2018).
6) A. M. Merzlikin, A. P. Vinogradov, M. Inoue, A. B. Khanikaev, and A. B. Granovsky, J. Magn. Magn. Mater. **300**, 108 (2006).
7) K. Fang, Z. Yu, V. Liu, and S. Fan, Opt. Lett. **36**, 4254 (2011).
8) V. I. Belotelov, L. L. Doskolovich, V. A. Kotov, E. A. Bezus, D. A. Bykov, and A. K. Zvezdin, Opt. Commun. **278**, 104 (2007).
9) V. I. Belotelov, L. L. Doskolovich, and A. K. Zvezdin, Phys. Rev. Lett. **98**, 077401 (2007).
10) V. I. Belotelov, D. A. Bykov, L. L. Doskolovich, A. N. Kalish, V. A. Kotov, and A. K. Zvezdin, Opt. Lett. **34**, 398 (2009).
11) E. Almpanis, P.-A. Pantazopoulos, N. Papanikolaou, V. Yannopapas, and N. Stefanou, J. Opt. Soc. Am. B **33**, 2609 (2016).
12) A. B. Khanikaev, A. V. Baryshev, A. A. Fedyanin, A. B. Granovsky, and M. Inoue, Opt. Express **15**, 6612 (2007).
13) A. B. Khanikaev, S. H. Mousavi, C. Wu, N. Dabidian, K. B. Alici, and G. Shvets, Opt. Commun. **285**, 3423 (2012).
14) A. B. Khanikaev et al., Nat. Commun. **7**, 12045 (2016).
15) A. V. Baryshev and A. M. Merzlikin, J. Opt. Soc. Am. B **33**, 1399 (2016).
16) S. Sakaguchi and N. Sugimoto, J. Lightwave Technol. **17**, 1087 (1999).
17) T. Yoshimoto, T. Goto, R. Isogai, Y. Nakamura, H. Takagi, C. A. Ross, and M. Inoue, Opt. Express **24**, 8746 (2016).
18) A. V. Baryshev, H. Uchida, and M. Inoue, J. Opt. Soc. Am. B **30**, 2371 (2013).
19) D. O. Ignatyeva, D. M. Krichevsky, V. I. Belotelov, F. Royer, S. Dash, and M. Levy, J. Appl. Phys. **132**, 100902 (2022).
20) A. I. Kuznetsov, A. E. Miroshnichenko, M. L. Brongersma, Y. S. Kivshar, and B. Luk'yanchuk, Science **354**, aag2472 (2016).
21) A. Christofi, Y. Kawaguchi, A. Alù, and A. B. Khanikaev, Opt. Lett. **43**, 1838 (2018).
22) T. Kiel, P. Varytis, B. Beverungen, P. T. Kristensen, and K. Busch, Opt. Lett. **46**, 1720 (2021).
23) S. Gao, Y. Ota, F. Tian, T. Liu, and S. Iwamoto, Opt. Express **31**, 13672 (2023).
24) D. O. Ignatyeva, D. Karki, A. A. Voronov, M. A. Kozhaev, D. M. Krichevsky, A. I. Chernov, M. Levy, and V. I. Belotelov, Nat. Commun. **11**, 5487 (2020).
25) S. Xia et al., ACS Photonics **9**, 1240 (2022).
26) J. M. Abendroth, M. L. Solomon, D. R. Barton, M. S. El Hadri, E. E. Fullerton, and J. A. Dionne, Adv. Optical Mater. **8**, 2001420 (2020).
27) M. G. Barsukova, A. S. Shorokhov, A. I. Musorin, D. N. Neshev, Y. S. Kivshar, and A. A. Fedyanin, ACS Photonics **4**, 2390 (2017).
28) Z. Wang and S. Fan, Appl. Phys. B **81**, 369 (2005).
29) D. Floess, J. Y. Chin, A. Kawatani, D. Dregely, H.-U. Habermeier, T. Weiss, and H. Giessen, Light: Sci. Appl. **4**, e284 (2015).
30) A. E. Miroshnichenko, S. Flach, and Y. S. Kivshar, Rev. Mod. Phys. **82**, 2257 (2010).
31) E. Melik-Gaykazyan, K. Koshelev, J.-H. Choi, S. S. Kruk, A. Bogdanov, H.-G. Park, and Y. Kivshar, Nano Lett. **21**, 1765 (2021).
32) C. W. Hsu, B. Zhen, A. D. Stone, J. D. Joannopoulos, and M. Soljačić, Nat Rev Mater **1**, 16048 (2016).
33) Y. Yang, I. I. Kravchenko, D. P. Briggs, and J. Valentine, Nat. Commun. **5**, 5753 (2014).
34) A. C. Overvig, S. C. Malek, M. J. Carter, S. Shrestha, and N. Yu, Phys. Rev. B **102**, 035434 (2020).
35) A. M. Chernyak, M. G. Barsukova, A. S. Shorokhov, A. I. Musorin, and A. A. Fedyanin, JETP Lett. **111**, 46 (2020).
36) M. Kerker, D.-S. Wang, and C. L. Giles, J. Opt. Soc. Am. **73**, 765 (1983).